



Cite this: *RSC Adv.*, 2017, 7, 33402

Received 25th May 2017  
Accepted 16th June 2017

DOI: 10.1039/c7ra05856j

rsc.li/rsc-advances

# Structural, mechanical and electronic properties of Nb<sub>2</sub>C: first-principles calculations†

Xiaojing Sha,  Namin Xiao, Yongjun Guan and Xiaosu Yi\*

Nb–C compounds are potential candidates to achieve high hardness and refractory nature. We performed a crystal structure search for the Nb–C system using an *ab initio* evolutionary algorithm implemented in the USPEX code. By comparing the formation enthalpy, a *P*–*x* phase diagram was calculated, and an orthorhombic *Pnnm* structure of Nb<sub>2</sub>C was predicted and denoted as Nb<sub>2</sub>C-*I*, which was both mechanically and dynamically stable. In this *Pnnm* phase, there are four-sided rings continuously along the *c*-axis, which probably contributes to the relatively high incompressibility of Nb<sub>2</sub>C-*I* along the crystallographic *c*-axis. Moreover, the hardness and Young's modulus were calculated to be 28.5 GPa and 448.9 GPa, respectively; hence, the Nb<sub>2</sub>C-*I* is considered as a potential ultra-stiff and hard material.

## 1 Introduction

In the past few decades, superhard materials with excellent mechanical properties have drawn extensive attention from the researchers and have been well-studied in terms of both theoretical and experimental aspects.<sup>1</sup> Traditional superhard materials, such as diamond,<sup>2,3</sup>  $\gamma$ -B,<sup>4</sup> *c*-BN,<sup>5</sup> and *c*-BC<sub>2</sub>N,<sup>6,7</sup> are mainly composed of light elements. Diamond, the earliest discovered and hardest (70–150 GPa) superhard material, shows promising mechanical properties and is hence among the most widely used superhard materials. However, diamond shows its own practical defects. At a temperature greater than 800 °C, diamond tends to oxidize. Moreover, when the diamond tool is used in the grinding or cutting of ferrous materials, the tool easily reacts with iron-based materials. The *c*-BN, another typical superhard material, is difficult to synthesise, which limits its practical application. Therefore, development of novel superhard multifunctional materials is an urgent requirement.

During the past decade, scientists were focused on the design of new materials in transition-metal (TM) light-element (LE) systems. One of the advantages of transition metals is their large bulk modulus. For example, the bulk modulus of Os is about 395–462 GPa,<sup>8</sup> which is close to that of diamond (446 GPa). However, the hardness of metal is always low, which is normally one-thirtieth that of diamond. This is mainly due to the huge difference of chemical bonds in the compound structures. Classical superhard materials usually hold three-dimensional networks composed of covalent bonds with sp<sup>3</sup> hybridization, which is the basis of superhard properties.

Therefore, the type of TM-LE bonding is the key factor for improving the hardness. Due to the behavior of high valence electron density and large interatomic distance, the transition metal can be intercalated with light elements, which may lead to the formation of covalent bonding between light elements and transition metals. Thus, the relatively high directional covalent bonds and valence electron density are considered to favor the formation of new superhard materials. It is believed that the carbides of the group-IV, -V, and -VI transition metals show an unusual combination of physical and chemical properties.<sup>9–14</sup> The transition-metal carbide (TMC) compounds combine the physical properties of three different kinds of materials: transition metals, covalent solids and ionic crystals,<sup>15</sup> making TMC a family of industrially relevant compounds with outstanding physical properties.

The niobium carbides are an emblematic TMC system, which exhibits meaningful physicochemical properties.<sup>10,16</sup> Moreover, niobium carbides are significant candidates for improving the mechanical properties of niobium alloys.<sup>10,16–19</sup> Niobium and carbide could form weak metallic or semi-conductors compounds with different compositions and space symmetries. In the Nb–C binary phase diagram, niobium carbides have four experimentally known compositions: NbC, Nb<sub>6</sub>C<sub>5</sub>, Nb<sub>4</sub>C<sub>3</sub>, and Nb<sub>2</sub>C.<sup>20–22</sup> Stoichiometric NbC is in the rocksalt structure,<sup>23</sup> in which Nb atoms form the cubic lattices, and C atoms occupy the octahedral interstitial positions. Nb<sub>4</sub>C<sub>3</sub> was reported to adopt a *R* $\bar{3}m$  space group, and Nb<sub>6</sub>C<sub>5</sub> is in the *P*3<sub>1</sub> space group.<sup>24,25</sup> Among all the niobium carbides, Nb<sub>2</sub>C is the least understood carbide;<sup>26</sup> it exists in three polymorphic forms:  $\gamma$ -Nb<sub>2</sub>C,  $\beta$ -Nb<sub>2</sub>C, and  $\alpha$ -Nb<sub>2</sub>C,<sup>27–31</sup> as reported in previous studies. The  $\gamma$ - and  $\beta$ -Nb<sub>2</sub>C are hexagonal phases. The  $\gamma$ -Nb<sub>2</sub>C is in L'3-type structure at temperatures above 2770 K. The  $\beta$ -Nb<sub>2</sub>C has  $\zeta$ -Fe<sub>2</sub>N structure at relatively low temperatures. The  $\alpha$ -Nb<sub>2</sub>C is an orthorhombic low temperature phase. As Hugosson reported,<sup>20</sup>

Materials Genome Center, Beijing Institute of Aeronautical Materials, Beijing, P. R. China. E-mail: yi\_xiaosu@sina.cn

† Electronic supplementary information (ESI) available. See DOI: 10.1039/c7ra05856j



some controversy exists in the determination of the structure of the orthorhombic phase. In his study, both structures showed energies of formation higher than those of the hexagonal phase. However, other studies showed that the formation energy of  $\alpha$ -Nb<sub>2</sub>C was the lowest, which indicated that the formation of  $\alpha$ -Nb<sub>2</sub>C was feasible.<sup>26,32</sup> To date, controversy still remains regarding the orthorhombic phase structure of Nb<sub>2</sub>C.

In this article, we performed a crystal structure search for the Nb–C system using an *ab initio* evolutionary algorithm implemented in the USPEX code. Full  $P$ - $x$  phase diagrams of the Nb–C system at 0 K were calculated. We report a new phase for Nb<sub>2</sub>C at high pressures. The predicted new phase of Nb<sub>2</sub>C belongs to the orthorhombic *Pnmm* space group. Moreover, this phase is dynamically and mechanically stable at ambient and high pressures. Through a detailed electronic structure analysis, we found that niobium and carbon formed strong bonds with sp<sup>3</sup> hybridization style, which further knitted into three-dimensional networks. Collectively, we proved that Nb<sub>2</sub>C can be a potential candidate for an ultra-stiff and hard material.

## 2 Methods

To search the stable and low-enthalpy structures of the Nb–C system, the evolutionary algorithm USPEX<sup>33–35</sup> coupled with an *ab initio* evolutionary algorithm (EA) was employed. The calculation was designed to find the most stable structure for the given stoichiometries under given external conditions as implemented in the USPEX code. In this study, evolutionary crystal structure prediction calculations were performed at 0, 10, 30, and 50 GPa for the Nb<sub>x</sub>C<sub>y</sub> system ( $x = 1–8, y = 1–8$ ) at zero temperature. We performed *ab initio* calculations with the local density approximation (LDA), as implemented in the Vienna *ab*

*initio* simulation package (VASP) code,<sup>36,37</sup> which is based on density functional theory. The electron–ion interaction was described *via* the projector augmented wave (PAW) scheme.<sup>38</sup> The orbitals 2s and 2p for C and 4p, 4d, and 5s for Nb were treated as valence states. During structural relaxation, a tested energy cutoff of 600 eV was used for the plane wave basis sets, and Monkhorst–Pack<sup>39</sup>  $k$ -point meshes with a resolution of 0.03 Å<sup>−1</sup> in the reciprocal space were used for all structures to minimize error from the  $k$ -point meshes. The atomic positions, lattice parameters, and cell volume were fully relaxed until the force on each atom was less than 1 meV Å<sup>−1</sup>. Phonons were calculated using the supercell method implemented in the PHONOPY package.<sup>40,41</sup> The strain–stress method was used to calculate the elastic constants. The shear modulus, bulk modulus, Young's modulus, and Pugh's indicator were derived from the Voigt–Reuss–Hill approximation.<sup>42–44</sup> The structure diagram of Nb<sub>2</sub>C was drawn using VESTA.<sup>45</sup>

## 3 Results and discussion

In this study, we uncovered a stable structure of Nb<sub>2</sub>C, denoted as Nb<sub>2</sub>C-*I*. At first, we calculated the formation enthalpy of Nb<sub>x</sub>C<sub>1−x</sub> using a fractional representation of Nb<sub>x</sub>C<sub>1−x</sub> with respect to its decomposition into Nb and C as

$$\Delta H(\text{Nb}_x\text{C}_{1-x}) = H(\text{Nb}_x\text{C}_{1-x}) - [x \times H(\text{Nb}) + (1-x) \times H(\text{C})]$$

where  $x$  is the concentration of Nb. The formation enthalpies from 0 to 50 GPa were evaluated as the difference in the enthalpy of the predicted Nb–C system with respect to Nb metal and C in their most stable forms (bcc phase for Nb and graphite for C), as depicted in Fig. 1. The formation enthalpy of NbC

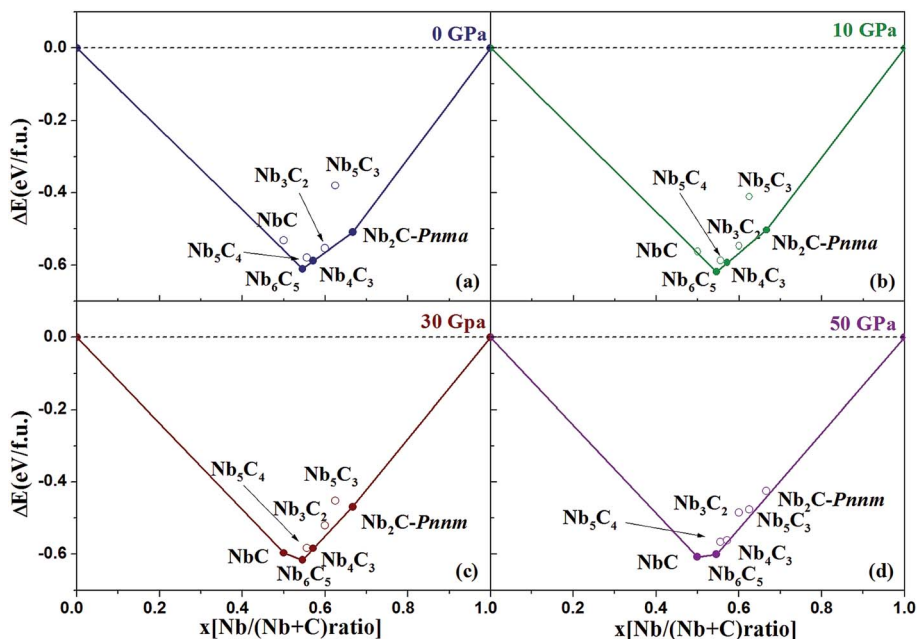


Fig. 1 Convex hull diagram for the Nb–C compounds. The formation enthalpies ( $\Delta H$ , with respect to Nb and C of their most stable phases) of Nb<sub>x</sub>C<sub>1−x</sub>. The abscissa  $x$  is the fraction of Nb in the structures. Circles on the solid lines represent stable ground-state compounds.



(*Fm3m*) in our calculation is  $-0.531$  eV, similar to the previous results<sup>20</sup> ( $-43$  mRy =  $-0.585$  eV). Structures lying on the convex hull are either thermodynamically stable or metastable and can be synthesized in principle. According to Fig. 1(a), at 0 GPa, the  $\text{Nb}_2\text{C-Pnma}$  and  $\text{Nb}_6\text{C}_5$  phases are thermodynamically stable, and  $\text{Nb}_4\text{C}_3$  is also located on the convex hull, which is similar to the previous results.<sup>32</sup> With an increase in the pressure, the stoichiometric NbC phase becomes thermodynamically stable, and  $\text{Nb}_2\text{C-Pnmm}$  is more stable than  $\text{Nb}_2\text{C-Pnma}$  at 30 GPa. We calculated the formation enthalpies of three candidates of  $\text{Nb}_2\text{C}$ . As Fig. 2 shows, the enthalpy curves of  $\text{Nb}_2\text{C}$  structures are presented. It can be clearly seen that the  $\text{Nb}_2\text{C-Pnma}$  is the most stable structure at 0 GPa, which is consistent with the Wu's studies.<sup>22</sup> When the pressure is greater than 15.8 GPa, the formation enthalpies of the proposed  $\text{Nb}_2\text{C-I}$  are lowest negative values, which indicates that  $\text{Nb}_2\text{C-I}$  is thermodynamically stable under pressure. From Fig. 1(d), it can be observed that at 50 GPa, the stable phases are only NbC and  $\text{Nb}_6\text{C}_5$ . We calculated the detailed enthalpy differences as a function of pressure. As shown in the ESI Fig. S1(a),† the enthalpy difference of NbC is calculated against decomposition into  $\text{Nb}_6\text{C}_5$  and C; thus, we concluded that the NbC phase becomes stable at 12.3 GPa. The enthalpy differences of  $\text{Nb}_4\text{C}_3$  and  $\text{Nb}_2\text{C-Pnmm}$  are calculated against decomposition into the constituent carbides. As shown in Fig. S1(b) and (c),† the structures of  $\text{Nb}_4\text{C}_3$  and  $\text{Nb}_2\text{C-Pnmm}$  become completely unstable at 39.7 GPa and 40.5 GPa, respectively. With these detailed calculations shown in Fig. S1,† a pressure–constituent ( $P$ - $x$ ) phase diagram of niobium carbide was constructed, which is plotted in Fig. 3. With the increase in C concentration, the Nb–C system first undergoes an orthorhombic to monoclinic transition and then transforms back to the cubic phase. Moreover, some phases of niobium carbides appear and decompose with the increase of pressure. However, the structure with high carbon concentration is not stable, even if the pressure is increased to 50 GPa.

The *Pnmm* structure, as we predicted, contains two  $\text{Nb}_2\text{C}$  in a unit cell at 20 GPa ( $a = 5.415$  Å,  $b = 4.837$  Å, and  $c = 3.019$  Å), in which two inequivalent atoms Nb and C occupy the Wyckoff

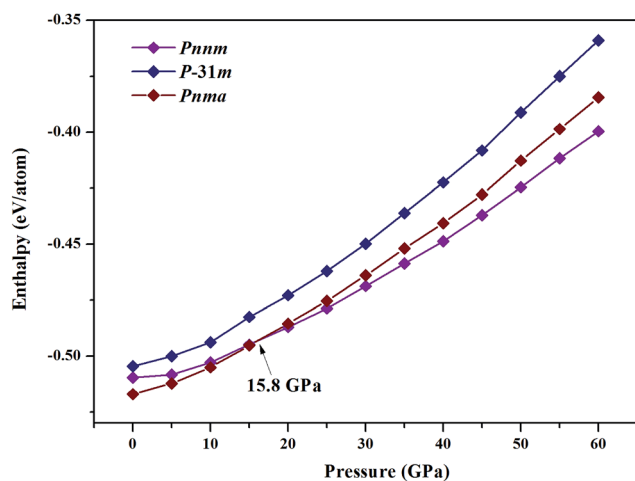


Fig. 2 Enthalpy–pressure diagrams. Calculated enthalpies as the function of pressure.

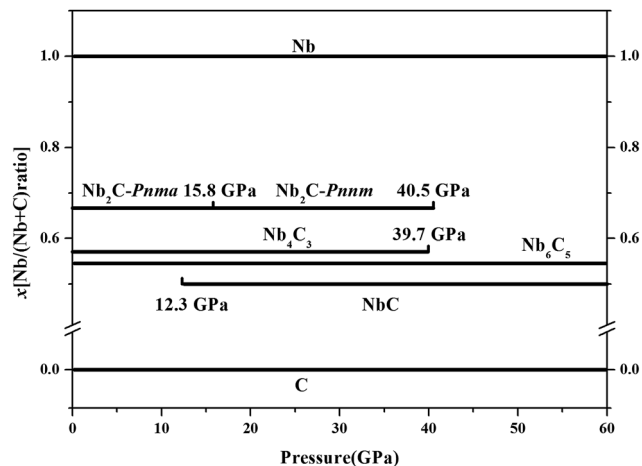


Fig. 3 Pressure–composition phase diagrams.

8h (0.3462, 0.7632, 0.5000) and 2b (0.5, 0.5, 0.0) sites, as summarized in Table 1 and shown in Fig. 4. Fig. 4(b) along the  $y$ -axis and Fig. 4(c) along the  $z$ -axis reveal a fundamental structure in the *Pnmm* phase. Fig. 4(d) shows the structure of *Pnma* phase along the  $y$ -axis. When we compared Fig. 4(b) with (d), it was observed that the carbon atoms in  $\text{Nb}_2\text{C-Pnmm}$  could help to achieve better formation of the three-dimensional space grid structure, which avoided the appearance of the interaction between metal atoms.

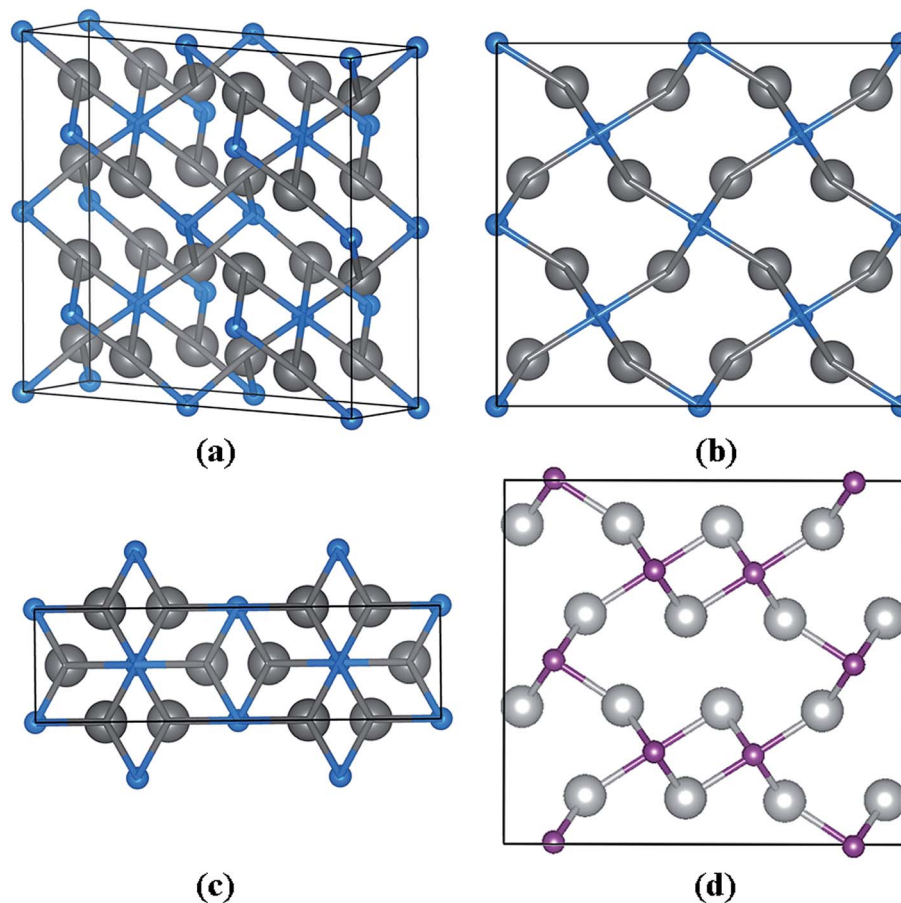
It is well-known that the phonon dispersion curves give information about the global structural stability of the materials. As shown in Fig. 5, we analyzed the phonon dispersion curves to test the lattice dynamical stability of  $\text{Nb}_2\text{C-I}$  at 0 and 20 GPa. The calculated phonon curves of  $\text{Nb}_2\text{C}$  have no soft mode in the Brillouin zone, indicating that  $\text{Nb}_2\text{C}$  is dynamically stable. For the purpose of understanding the mechanical properties, the elastic constants are deemed essential. The elastic constants  $C_{ij}$  of the *Pnmm* phases are listed in Table 2. For the proposed  $\text{Nb}_2\text{C-Pnmm}$ , all  $C_{ij}$  satisfy Born–Huang criteria,<sup>46</sup> which means that the proposed  $\text{Nb}_2\text{C-Pnmm}$  is mechanically stable. We determined that the  $\text{Nb}_2\text{C-Pnmm}$  could be synthesized under high pressure and preserved under ambient pressure. From Table 2, it can be found that the calculated  $C_{33}$  value is bigger than the values of  $C_{11}$  and  $C_{22}$ , indicating that there is relatively high incompressibility along the  $c$ -axis. The relative high incompressibility of the proposed  $\text{Nb}_2\text{C}$  along the  $c$ -axis is perhaps contributed by the existence of four-sided rings, which are continuously along the crystallographic  $c$ -axis. In contrast, four-sided rings and eight-sided rings exist alternately along the  $b$ -axis or  $c$ -axis. Therefore, there is certain disparity between  $C_{33}$  and  $C_{11}$  (or  $C_{22}$ ).

It is well-known that superhard materials should have high bulk modulus and high shear modulus to resist the volume change and shape change. At 0 and 20 GPa, the bulk modulus of  $\text{Nb}_2\text{C-Pnmm}$  is 244 and 310 GPa, respectively, which are larger than the values of  $\text{Nb}_2\text{C-Pnma}$  (236 and 304 GPa, respectively). Because the value of the bulk modulus is large,  $\text{Nb}_2\text{C}$  can be grouped into incompressible materials. As reported in Table 2,



**Table 1** The optimized equilibrium lattice constants  $a$ ,  $b$ , and  $c$  (Å), and atomic coordinates for Nb<sub>2</sub>C- $I$  at 20 GPa

Structure	Parameters (Å)	Atom	$x$	$y$	$z$	
Nb <sub>2</sub> C	$Pn\bar{m}$ (orthorhombic)	$a = 5.415, b = 4.837, c = 3.019$	Nb(8h)	0.3462	0.7632	0.5000
			C(2b)	0.5000	0.5000	0.0000

**Fig. 4** Crystal structures of the predicted Nb<sub>2</sub>C- $Pn\bar{m}$ . (a) The structure of Nb<sub>2</sub>C- $Pn\bar{m}$ . (b) The structure along the  $y$ -axis. (c) Along the  $z$ -axis. The large gray and small blue spheres represent the Nb and C atoms, respectively. (d) The structure of Nb<sub>2</sub>C- $Pnma$  along the  $y$ -axis.

the Poisson's ratio  $\nu$  of Nb<sub>2</sub>C- $Pn\bar{m}$  is about 0.19. Usually, strong directionality degree of covalent bonding is considered in the materials when the  $\nu$  value is near 0.2, indicating that the directionality degree of covalent bonding of Nb<sub>2</sub>C- $Pn\bar{m}$  is strong. The Pugh's indicator  $G/B$  of Nb<sub>2</sub>C is 0.77, which is a relatively large value. According to the Pugh's modulus ratio defined by Cheng *et al.*,<sup>47</sup> the Nb<sub>2</sub>C- $I$  phase is a brittle and hard material with a huge capability to resist elastic plastic deformation. To gain a more comprehensive and profound understanding of the mechanical property, we calculated the Vickers hardness of Nb<sub>2</sub>C- $I$ . The Vickers hardness  $H_V$ , estimated by the empirical model, was obtained by the following formula:

$$H_V = (k^2 G)^{0.585} - 3 \quad (k = G/B)$$

The calculated hardness of Nb<sub>2</sub>C- $I$  is 28.5 GPa, which almost matches that of the hard material WC (21.5–33.4 GPa).<sup>47,48</sup> Our

results suggested that the proposed Nb<sub>2</sub>C- $I$  could be a potential candidate for ultra-stiff and hard materials.

The electronic structure is crucial to understand the origin of physical properties of these carbides. The total and site projected electronic densities of states (PDOS) of Nb<sub>2</sub>C- $I$  are shown in Fig. 6(a). As the graphic shows, Nb<sub>2</sub>C is a metal as the d electronics of Nb are mainly attributed to the density near the Fermi energy in our calculation model. To determine the hybridization between C and Nb, projected electronic densities of states of the nearest Nb and C are calculated, as shown in Fig. 6(b). There is an obvious hybridization between C 2p and Nb 4d states, which is a common feature of typical TMC superhard materials. To obtain more information about the bonding character, the electronic localization function (ELF) of Nb<sub>2</sub>C- $I$  was calculated, as shown in Fig. 7. The electron localization function between Nb atoms and C atoms has a slight increase as compared to that in the background, which



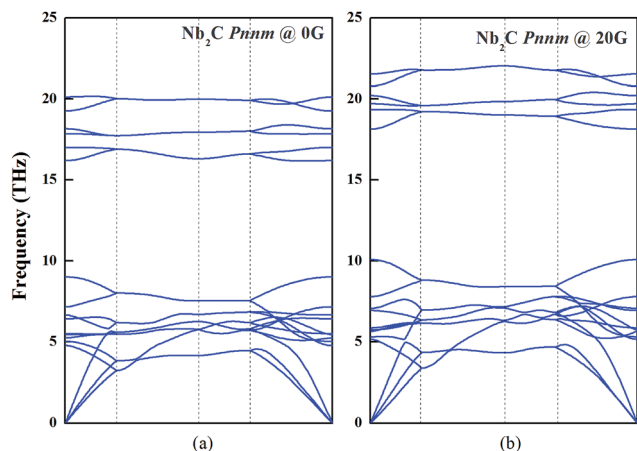


Fig. 5 Dynamic stability of  $\text{Nb}_2\text{C-I}$ . The phonon dispersion curves of  $\text{Nb}_2\text{C-I}$  along the high symmetry directions of the Brillouin zone at 0 and 20 GPa.

Table 2 Elastic constants  $C_{ij}$ , Poisson's ratio  $\nu$ , bulk modulus  $B$  (GPa), shear modulus  $G$  (GPa), Pugh's indicator  $G/B$ , Young's modulus  $E$  (GPa), and Vickers hardness  $H_V$  of  $\text{Nb}_2\text{C-Pnma}$  and  $\text{Nb}_2\text{C-Pnnm}$  at 0 GPa

	$C_{11}$	$C_{22}$	$C_{33}$	$C_{44}$	$C_{55}$	$C_{66}$	$C_{12}$	$C_{13}$	$C_{23}$
<i>Pnma</i>	390	405	390	76	119	122	157	129	136
<i>Pnnm</i>	383	389	415	101	102	137	156	153	127
	$\nu$	$B$	$G$	$G/B$	$E$	$H_V$			
<i>Pnma</i>	0.19	236.1	178.1	0.75	426.9	26.8			
<i>Pnnm</i>	0.19	244.5	188.0	0.77	448.9	28.5			

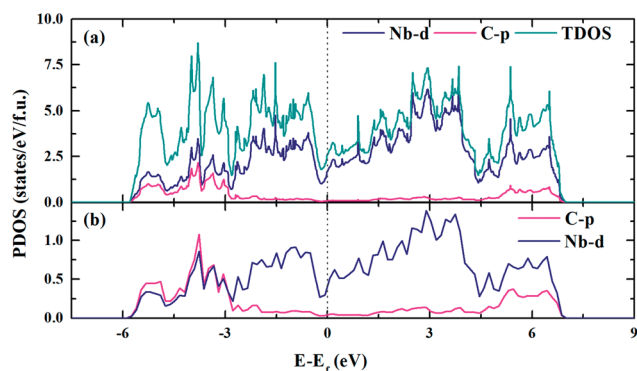


Fig. 6 Electronic density of states of  $\text{Nb}_2\text{C-I}$ . The DOS (a) and PDOS (b) of  $\text{Nb}_2\text{C-I}$ . The vertical black dashed line denotes the Fermi level.

indicates that mixed bonds between the two atoms are present in this area, in which the ionic bonds are dominant. As Becke defined,<sup>49</sup> the electrons can move freely in the areas of  $\text{ELF} = 0.5$ . In Fig. 7(a), the green region is almost connected. However, there are disconnected equivalent spheres in Fig. 7(b). In total, the equivalent sphere of  $\text{ELF} = 0.5$  is

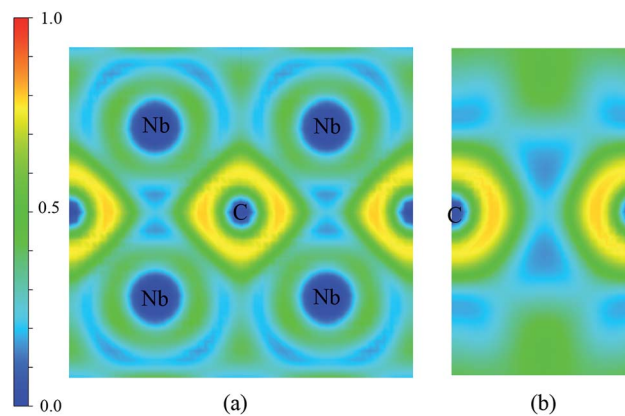


Fig. 7 Contours of the electronic localization functions (ELF). Electron localization function isosurface maps for (a) Miller indices: (1.67 1 0) and (b) Miller indices: (1 0 0).

partially connected in the whole crystal, which may enhance the weak metallicity properties.

## 4 Summary

In summary, we researched the full-scale zero-temperature Nb–C phase diagram using an *ab initio* evolutionary algorithm implemented in the USPEX code. The  $P$ – $x$  phase diagrams of the Nb–C system are constructed. A new structure of  $\text{Nb}_2\text{C}$  has been uncovered and denoted as  $\text{Nb}_2\text{C-I}$ . The  $\text{Nb}_2\text{C-I}$  belongs to the orthorhombic system with the space group *Pnnm*. Phase stability, mechanical properties, and electronic properties of  $\text{Nb}_2\text{C-I}$  were investigated. The Vickers hardness and Young's modulus of  $\text{Nb}_2\text{C-I}$  have been calculated to be 28.5 GPa and 448.9 GPa, respectively, which prove that  $\text{Nb}_2\text{C-I}$  can be considered as low compressible materials. We considered that the formation of continuous four-sided rings along the  $c$ -axis might cause high incompressibility of  $\text{Nb}_2\text{C-I}$  in the  $c$ -axis direction. A deep analysis of the electronic density of states and chemical bonding indicates that an ionic bond is dominant in the  $\text{Nb}_2\text{C}$  crystals.

## Acknowledgements

This work was supported by the National Key Research and Development Program of China (No. 2016YFB0700505, 2016YFB0701401). Parts of the results described in this paper are obtained on the Era of Computer Network Information Center of Chinese Academy of Sciences.

## References

- 1 V. V. Brazhkin, A. G. Lyapin and R. J. Hemley, *Philos. Mag. A*, 2002, **82**, 231–253.
- 2 N. Mounet and N. Marzari, *Phys. Rev. B: Condens. Matter Mater. Phys.*, 2005, **71**, 205214.
- 3 V. Brazhkin, N. Dubrovinskaia, A. Nicol, N. Novikov, *et al.*, *Nat. Mater.*, 2004, **3**, 576–577.



- 4 J. Qin, N. Nishiyama, H. Ohfuji, *et al.*, *Scr. Mater.*, 2012, **67**(3), 257–260.
- 5 J. C. Zheng, *Phys. Rev. B: Condens. Matter Mater. Phys.*, 2005, **72**, 052105.
- 6 V. L. Solozhenko, D. Andrault, T. G. Figue, *et al.*, *Appl. Phys. Lett.*, 2001, **78**(10), 1385–1387.
- 7 Z. Pan, H. Sun and C. Chen, *Phys. Rev. Lett.*, 2007, **98**(13), 135505.
- 8 F. Occelli, D. L. Farber, J. Badro, *et al.*, *Phys. Rev. Lett.*, 2004, **93**(9), 095502.
- 9 W. Weber, *Phys. Rev. B: Solid State*, 1973, **8**, 11.
- 10 L. E. Toth, *Transition Metal Carbides and Nitrides*, Academic Press, New York, 1971.
- 11 S. T. Oyama, *Catal. Today*, 1992, **15**, 179.
- 12 Z. Zhao, K. Bao, F. Tian, D. Duan, B. Liu and T. Cui, *Phys. Rev. B: Condens. Matter Mater. Phys.*, 2016, **93**, 214104.
- 13 Y. Liang, J. Yang, X. Yuan, W. Qiu, Z. Zhong, J. Yang and W. Zhang, *Sci. Rep.*, 2014, **4**, 5063.
- 14 S. Wang, D. Antonio, X. Yu, J. Zhang, A. L. Cornelius, D. He and Y. Zhao, *Sci. Rep.*, 2015, **5**, 13733.
- 15 H. Hwu and J. G. Chen, *Chem. Rev.*, 2005, **105**, 185–212.
- 16 E. K. Storms, *The Refractory Carbides*, Academic Press, New York-London, 1967.
- 17 E. J. Delgrosso, C. E. Carlson and J. J. Kaminsky, *J. Less-Common Met.*, 1967, **12**, 173.
- 18 F. C. Campbell, *Elements of Metallurgy and Engineering Alloys*, ASM International, Ohio, 2008.
- 19 V. Javaheri, F. Shahri, M. Mohammadnezhad, M. Tamizifar and M. Naseri, *J. Mater. Eng. Perform.*, 2014, **23**, 3558–3566.
- 20 H. W. Hugosson, O. Eriksson, U. Jansson and B. Johansson, *Phys. Rev. B: Condens. Matter Mater. Phys.*, 2001, **63**, 134108.
- 21 H. W. Hugosson, U. Jansson, B. Johansson and O. Eriksson, *Chem. Phys. Lett.*, 2001, **333**, 444–450.
- 22 L. Wu, Y. Wang, Z. Yan, J. Zhang, F. Xiao and B. Liao, *J. Alloys Compd.*, 2013, **561**, 220–227.
- 23 H. M. Ledbetter, S. Chevacharoenkul and R. F. Davis, *J. Appl. Phys.*, 1986, **60**, 1614–1617.
- 24 A. N. Christensen, *Acta Chem. Scand., Ser. A*, 1985, **39**, 803–804.
- 25 K. Yvon and E. Parthé, *Acta Crystallogr., Sect. B: Struct. Sci.*, 1970, **26**, 149–153.
- 26 B. Vishwanadh, T. S. R. C. Murthy, A. Arya, R. Tewari and G. K. Dey, *J. Alloys Compd.*, 2016, **671**, 424–434.
- 27 J. F. Smith, O. N. Carlson and D. R. R. Avillez, *J. Nucl. Mater.*, 1987, **148**, 1–16.
- 28 E. Parthe and K. Yvon, *Acta Crystallogr., Sect. B: Struct. Sci.*, 1970, **26**, 153–163.
- 29 E. Rudy and C. E. Brukl, *J. Am. Ceram. Soc.*, 1967, **50**, 265–268.
- 30 N. Terao, *Jpn. J. Appl. Phys.*, 1964, **104**, 104–111.
- 31 B. Lonnberg and T. Lundstrom, *J. Less-Common Met.*, 1985, **113**, 261–268.
- 32 X. Yu, C. R. Weinberger and G. B. Thompson, *Comput. Mater. Sci.*, 2016, **112**, 318–326.
- 33 A. R. Oganov and C. W. Glass, *J. Chem. Phys.*, 2006, **124**, 244704.
- 34 A. R. Oganov, C. W. Glass and S. Ono, *Earth Planet. Sci. Lett.*, 2006, **241**, 95–103.
- 35 C. W. Glass, A. R. Oganov and N. Hansen, *Comput. Phys. Commun.*, 2006, **175**, 713–720.
- 36 G. Kresse and D. Joubert, *Phys. Rev. B: Condens. Matter Mater. Phys.*, 1999, **59**, 1758–1775.
- 37 G. Kresse and J. Furthmuller, *Phys. Rev. B: Condens. Matter Mater. Phys.*, 1996, **54**, 11169–11186.
- 38 P. E. Bloch, *Phys. Rev. B: Condens. Matter Mater. Phys.*, 1994, **50**, 17953–17979.
- 39 H. J. Monkhorst and J. D. Pack, *Phys. Rev. B: Solid State*, 1976, **13**, 5188–5192.
- 40 A. Togo, F. Oba and I. Tanaka, *Phys. Rev. B: Condens. Matter Mater. Phys.*, 2008, **78**, 134106.
- 41 A. Togo, *Phonopy*, <https://atztogo.github.io/phonopy/>.
- 42 R. Hill, *Proc. Phys. Soc., London, Sect. A*, 1952, **65**, 349–354.
- 43 *Lehrbuch der kristallphysik*, ed. W. Voigt, Teubner-Leipzig, New York, Macmillan, 1928, p. 739.
- 44 A. Reuss, *Z. Angew. Math. Phys.*, 1929, **9**, 49–58.
- 45 K. Momma and F. Izumi, *J. Appl. Crystallogr.*, 2011, **44**, 1272–1276.
- 46 Z. Wu, E. Zhao, H. Xiang, X. Hao, X. Liu and J. Meng, *Phys. Rev. B: Condens. Matter Mater. Phys.*, 2007, **76**, 054115.
- 47 X. Cheng, H. Niu, D. Li and Y. Li, *Intermetallics*, 2011, **19**, 1275–1281.
- 48 A. Simunek and J. Vackar, *Phys. Rev. Lett.*, 2006, **96**, 085501.
- 49 A. D. Becke and K. E. Edgecombe, *J. Chem. Phys.*, 1990, **92**, 5397.

